(Received 7 April 2025, Accepted 23 May 2025, Scheduled 3 June 2025)

Compact Slow-Wave Folded Substrate Integrated Waveguide with Broadband and Low-Loss Performance

Liang Li[1,3,*], Yangping Zhao[2], Shunli Hong[1,3], and Minjin Zhang[4]

[1]School of Intelligent Transportation of Zhejiang Institute of Communications, Hangzhou 311112, Zhejiang, China
[2]College of Civil and Transportation Engineering of Shenzhen University, Shenzhen 518060, Guangdong, China
[3]Zhejiang Province Engineering Research Center for Applied Technology of Digital Highways, Hangzhou 311112, Zhejiang, China
[4]Jiangsu Brmicro Microelectronics Co., Ltd. No. 1699, South Zuchongzhi Road, Kunshan 215316, Jiangsu, China

ABSTRACT: This paper presents a novel compact, broadband, and low-loss slow-wave folded substrate integrated waveguide (SW-FSIW) structure, achieved by integrating grounded patches into a conventional FSIW configuration. The slow-wave effect is generated through enhanced capacitive coupling between the grounded patches and the signal trace grid patterned on the FSIW's middle metal layer. Compared to a conventional SIW with the same cutoff frequency, the SW-FSIW achieves a 66% reduction in lateral dimension and a 37% reduction in longitudinal dimension, resulting in a total area reduction of 78.6%. The design exhibits superior performance to state-of-the-art slow-wave SIWs in lateral size reduction, fractional bandwidth (92%), and attenuation constant. Experimental validation shows excellent agreement between measurements and simulations for a fabricated prototype operating across the 4.07–11 GHz frequency range, confirming the structure's strong potential for applications in compact microwave systems, 5G/6G front-ends, and satellite communications.

1. INTRODUCTION

Substrate integrated waveguide (SIW) [1, 2] has been widely used in microwave circuits and systems, due to its advantages of low loss, low cost, planar integration, high power capacity, and robust electromagnetic (EM) shielding. Despite these advantages, conventional SIWs face inherent limitations in compactness due to their high-pass characteristics, particularly in low-frequency applications (< 10 GHz). Recent advances in SIW miniaturization have primarily focused on structural modifications, including folded SIW (FSIW) configurations [3, 4], half-mode SIW (HMSIW) implementations [5–7], and ridged SIW (RSIW) designs [8–11]. While these approaches successfully reduce lateral dimensions, they fail to address the critical need for longitudinal size reduction, ultimately limiting their effectiveness in space-constrained applications.

Recently, the introduction of slow-wave (SW) techniques has opened new possibilities for comprehensive SIW miniaturization. Pioneering work employing metallized blind via-hole arrays [12] demonstrated 40% reduction in both lateral and longitudinal dimensions. Subsequent developments, including multi-antipodal via-holes with distributed metal strips [13], improved it to 55% lateral and 50% longitudinal reduction, while alternative designs combining via-holes with shorted patches [14] achieved 53% lateral and 73% longitudinal reduction. However, these approaches share significant drawbacks including complex fabrication processes and elevated production costs associated with metallized blind via-hole implementation. Alternatively, single-layer SW-SIWs have been developed using microstrip polylines [15] or lumped inductors [16]. These methods leverage increased effective permeability/permittivity to achieve $\sim 40\%$ size reduction. In addition, slow-wave HMSIW (SW-HMSIW) variants [17–19] have been proposed, but their semi-open structures compromise EM shielding and introduce undesirable radiation losses.

In this work, we propose a novel compact, broadband, and low-loss SW-FSIW structure. The proposed design incorporates grounded patches within a conventional FSIW configuration, where the slow-wave effect is achieved through enhanced capacitive coupling between these patches and the signal trace grid on the middle metal layer. The proposed structure is inspired by the SW-HMSIW design reported in [20], which utilizes a mushroom-like structure for miniaturization.

Compared to state-of-the-art slow-wave SIW implementations, the SW-FSIW demonstrates three key advancements: it achieves the most significant lateral size reduction to date (66%), maintains the widest fractional bandwidth (92%) while exhibiting the lowest attenuation characteristics, and does so at a moderate fabrication cost that avoids the complexities associated with metallized blind via-holes. The effectiveness of this approach is validated through both simulation and experimental measurements of a fabricated prototype operating across the 4.07–11 GHz frequency range, with results showing excellent agreement between theoretical predictions and practical performance.

The remainder of this paper is organized as follows. Section 2 presents the operational principles and design methodology. Section 3 provides simulation and measurement results, and Section 4 concludes the paper.

* Corresponding author: Liang Li (liliang@zjvtit.edu.cn).

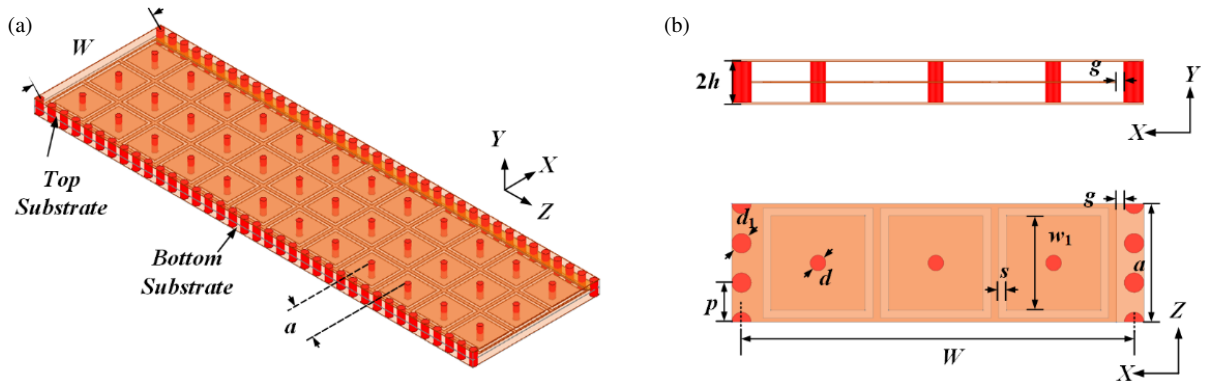

FIGURE 1. Configuration of the proposed SW-FSIW. (a) 3-D view. (b) Unit length.

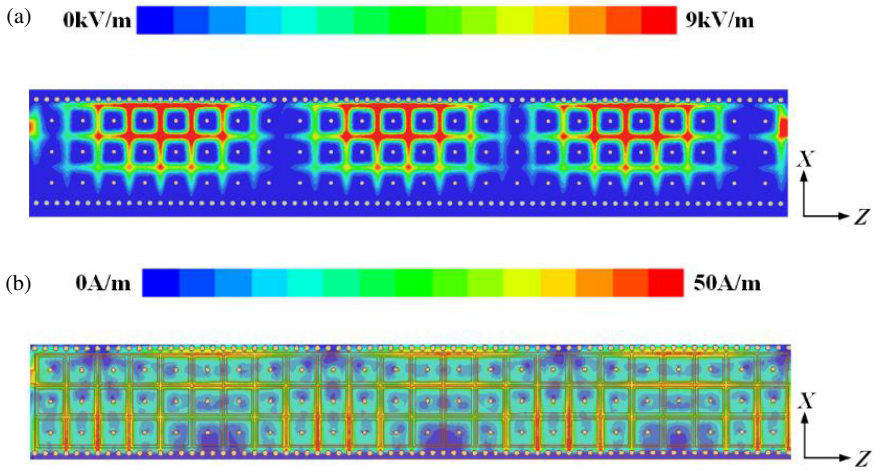

FIGURE 2. Top view of the EM field distributions of the SW-FSIW at 5 GHz. (a) Electric field. (b) Magnetic field.

2. DESIGN OF THE SW-FSIW

2.1. Configuration and Electromagnetic Field Analysis

The proposed SW-FSIW configuration is illustrated in Figure 1. The structure utilizes two layers of Taconic TLY-5 substrate with dielectric constant $\varepsilon_r = 2.2$, loss tangent tan $\delta = 0.0009$, and thickness $h = 0.508$ mm. The waveguide's lateral dimension (W) is defined by two rows of metallized via-holes connecting the top and bottom ground planes. The diameter of the metallized via-holes is d_1, and the pitch between two adjacent via-holes is p. The critical gap width g between the middle metal layer and via-hole wall follows the theoretical formulation established in [3]. Each periodic unit of the SW-FSIW, shown in Figure 1(b), incorporates three innovative ring-mushroom elements. These elements consist of square patches (width w_1) on the middle metal layer, vertically interconnected to both ground planes through metalized via-holes. Each patch is concentrically surrounded by a square slot (width s) and an outer metal grid. The square slots serve as distributed capacitors between grounded patches and the metal grid, enhancing the shunt capacitance of the FSIW without significantly affecting the series inductance. As a result, the effective permittivity (ε_{reff}) is increased while the effective permeability is unchanged.

The cutoff frequency of the SW-FSIW is given by [12]:

$$f_{c\_SW\text{-}FSIW} = \frac{c_0}{4W_{F\_eff}\sqrt{\varepsilon_{r\_eff}}} = \sqrt{\frac{\varepsilon_r}{\varepsilon_{r\_eff}}} f_{c\_FSIW}, \tag{1}$$

where c_0 is the speed of light in free space, and $W_{\text{F\_eff}}$ is the effective width of the FSIW.

The phase velocity (v_p) of the SW-FSIW can be expressed as:

$$v_p = \frac{c_0}{\sqrt{\varepsilon_{r\_eff}\left(1 - \left(\frac{f_{c\_SW\text{-}FSIW}}{f}\right)^2\right)}} \tag{2}$$

Then, the guided wavelength (λ_g) is calculated by

$$\lambda_g = v_p / f \tag{3}$$

Equations (1)–(3) demonstrate that the cutoff frequency, phase velocity, and guided wavelength are reduced with the increase of effective permittivity (ε_{r_eff}). This results in the desired slow-wave effect.

Full-wave simulations conducted in Ansys HFSS reveal the distinctive electromagnetic field distribution at 5 GHz (Figures 2–3). The electric field shows strong concentration within the square slots, such concentration indicates a substantial enhancement of the shunt capacitance. On the other hand, the

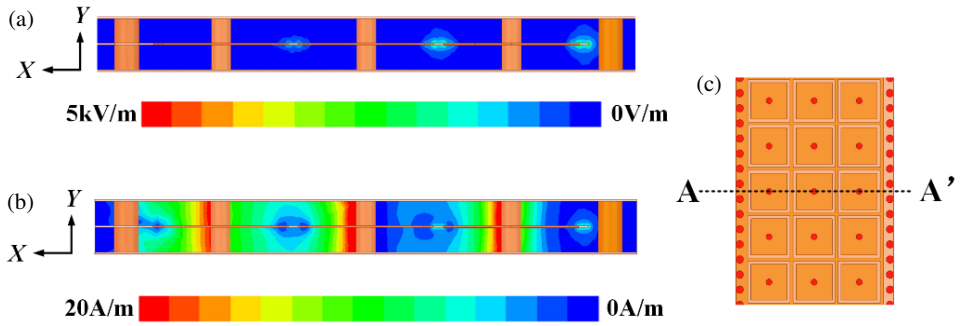

FIGURE 3. Cross-section view of the EM field distributions of the SW-FSIW at 5 GHz. (a) Electric field. (b) Magnetic field. (c) Cross-sectional position.

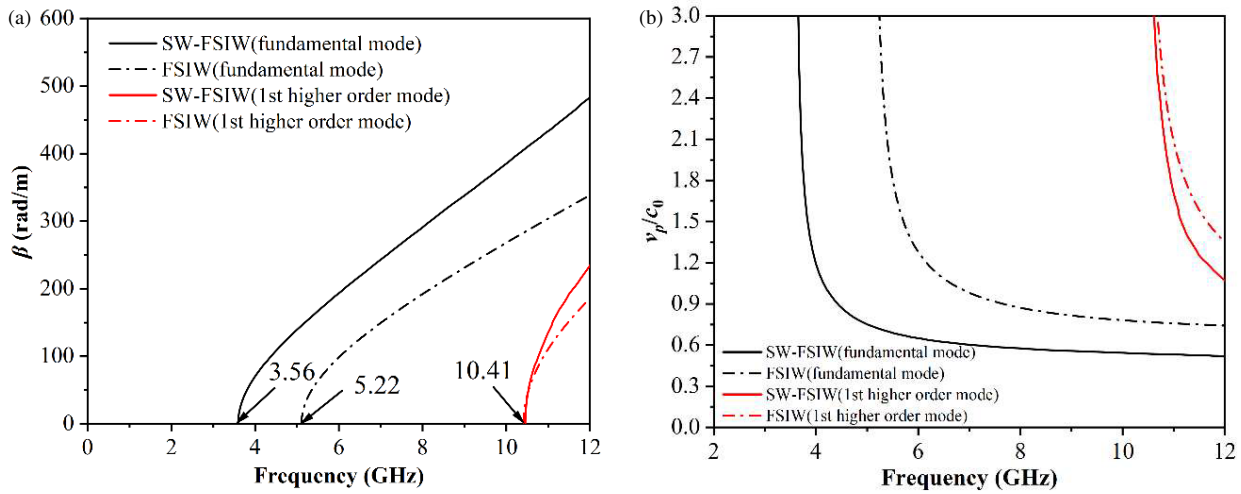

FIGURE 4. (a) Simulated phase constant and (b) normalized phase velocity of the SW-FSIW and FSIW with the same lateral width.

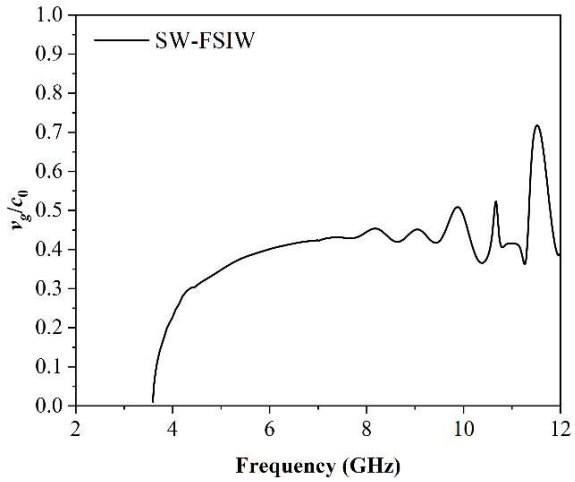

FIGURE 5. Simulated normalized group velocity of the SW-FSIW.

magnetic field distributes throughout the whole volume. This spatial separation of electric and magnetic fields characterizes effective slow-wave propagation.

Comparative analysis of dispersion characteristics (Figure 4) demonstrates the SW-FSIW's superior performance. The structure achieves a 3.56 GHz cutoff frequency compared to 5.22 GHz for conventional FSIW, enabling a 32% lateral width reduction versus FSIW (equivalent to 66% reduction compared to standard SIW). Additionally, the normalized phase velocity (v_p/c_0) decreases to 0.55 at 8 GHz (versus 0.87 for FSIW), corresponding to a 37% longitudinal dimension reduction. Collectively, these improvements yield a remarkable 78.6% total area reduction compared to conventional SIW implementations. Figure 4 also demonstrates that the SW-FSIW achieves a significantly wider single-mode operation bandwidth (3.56–10.41 GHz, 98.1%) than the conventional FSIW (5.22–10.41 GHz, 66.4%). This performance advantage stems from their distinct higher-order mode characteristics: the SW-FSIW's first higher-order mode is the folded TE30 mode, while the FSIW exhibits a folded TE20 mode as its first higher-order mode. Figure 5 demonstrates that the proposed SW-FSIW achieves a reduced group velocity ($v_g \approx 0.4c$) from 4 to 11 GHz, confirming its effective slow-wave operation. Furthermore, the flat group velocity across 6–11 GHz confirms the low-dispersion characteristics of the proposed structure.

2.2. Parametric Analysis

Figure 6 presents the phase constant and phase velocity characteristics of the SW-FSIW structure versus the number of elements. Both cutoff frequency and phase velocity exhibit an inverse relationship with the number of elements. A notable per-

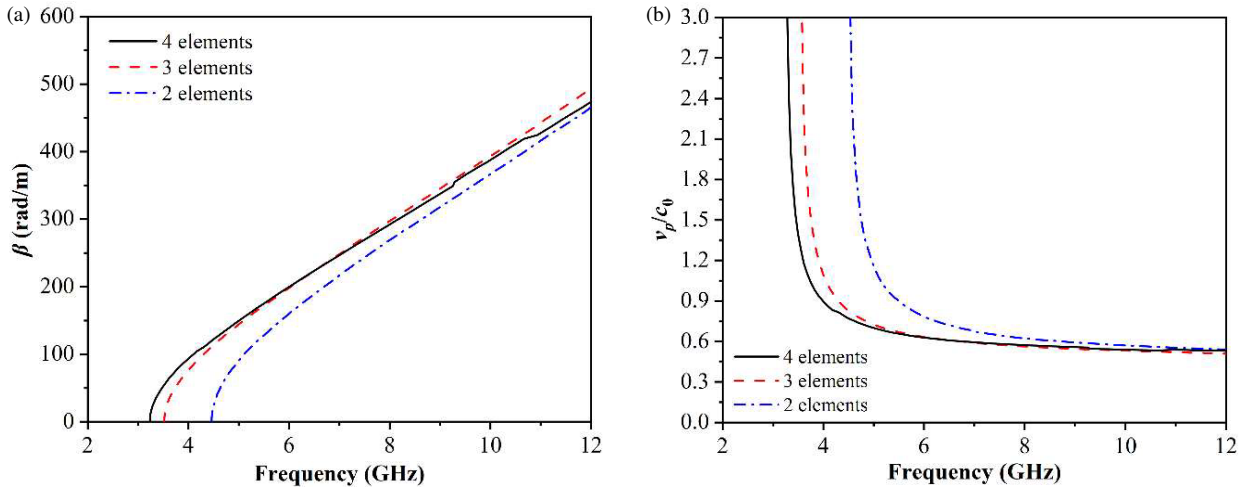

FIGURE 6. (a) Simulated phase constant and (b) normalized phase velocity of the SW-FSIW versus the number of elements.

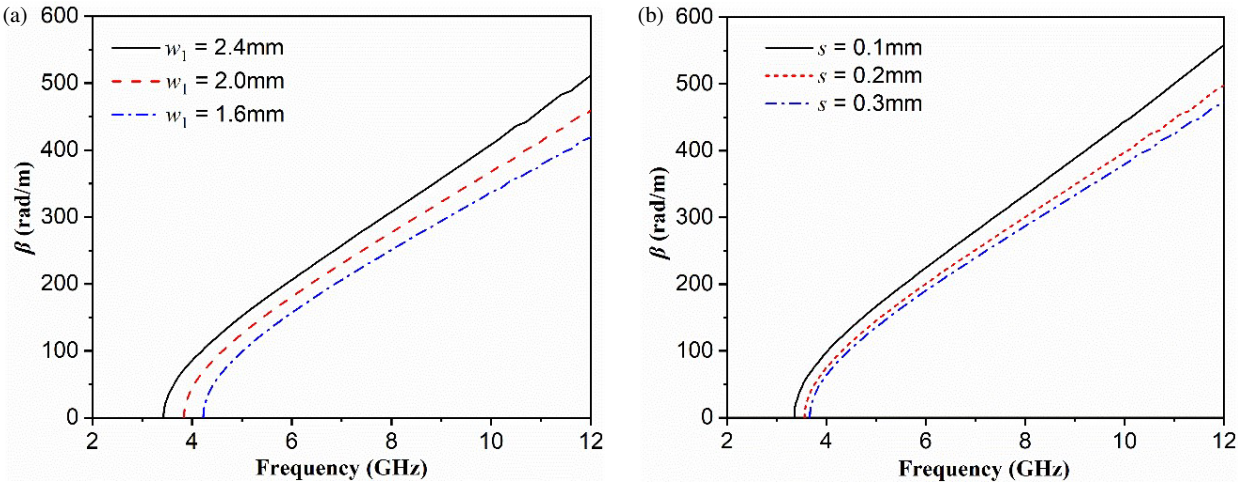

FIGURE 7. Simulated phase constant of the SW-FSIW with different values of (a) w_1 and (b) s.

formance shift occurs between 2-element and 3-element configurations, while the transition to 4 elements yields diminishing returns. Based on these observations and accounting for the trade-off between performance gains and structural complexity, 3-element configuration was adopted as a compromise between electrical performance and practical implementation.

The equivalent permittivity of the SW-FSIW structure exhibits strong dependence on two key geometric parameters: the grounded patch width (w_1) and slot width (s). To systematically investigate their influence on waveguide performance, we conducted a comprehensive parametric study while maintaining other dimensions constant ($h = 0.508$ mm, $s = 0.2$ mm, $w_1 = 2.4$ mm, $g = 0.2$ mm, $W = 10$ mm, and $d_2 = 0.4$ mm).

Figure 7 presents the relationship between these parameters and the cutoff frequency. The simulation results demonstrate an inverse correlation between cutoff frequency and both patch width and slot width — the cutoff frequency decreases as w_1 increases or s decreases. This trend becomes physically intuitive when considering the underlying capacitance mechanism: wider patches provide greater surface area for charge accumulation, while narrower slots enhance electric field concentration between adjacent metal features, both contributing to increased distributed capacitance. An identical parametric dependence emerges in the normalized phase velocity characteristics shown in Figure 8. The phase velocity decreases proportionally with increasing w_1 or decreasing s, confirming the consistent enhancement of slow-wave effects through these geometric modifications. This dual-parameter sensitivity provides valuable design flexibility, as the cutoff frequency and phase velocity can be independently tuned by appropriate adjustment of patch and slot dimensions.

From an application perspective, these parametric relationships enable precise control over both lateral and longitudinal waveguide dimensions. The reduction in cutoff frequency permits decreased lateral width while maintaining operational bandwidth, and the lowered phase velocity allows proportional reduction in longitudinal dimensions. This dual-dimensional scaling capability is particularly valuable for compact microwave system design, where simultaneous optimization of both planar dimensions is often required.

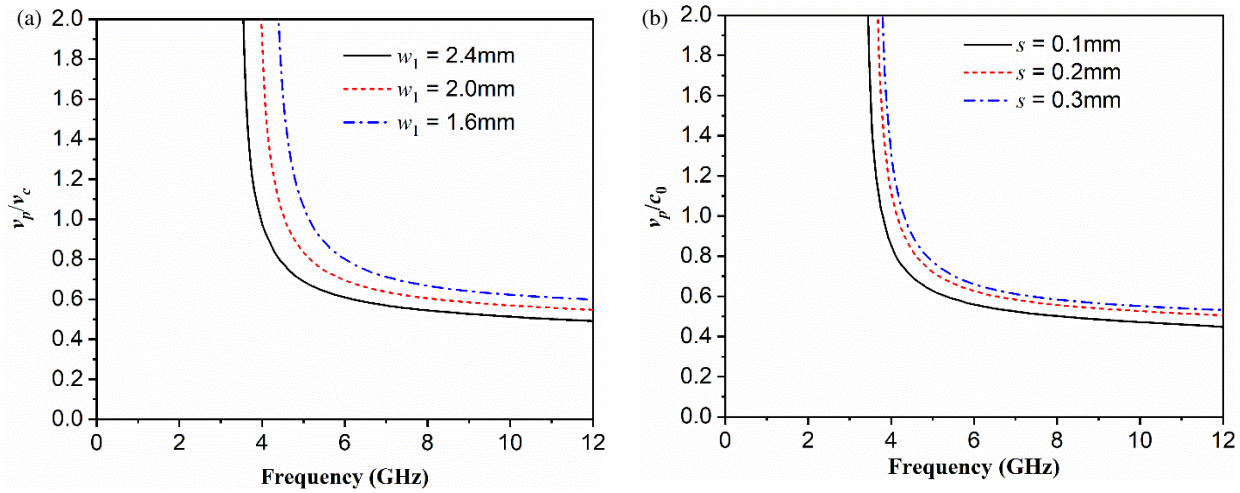

FIGURE 8. Simulated normalized phase velocity of the SW-FSIW with different values of (a) w_1 and (b) s.

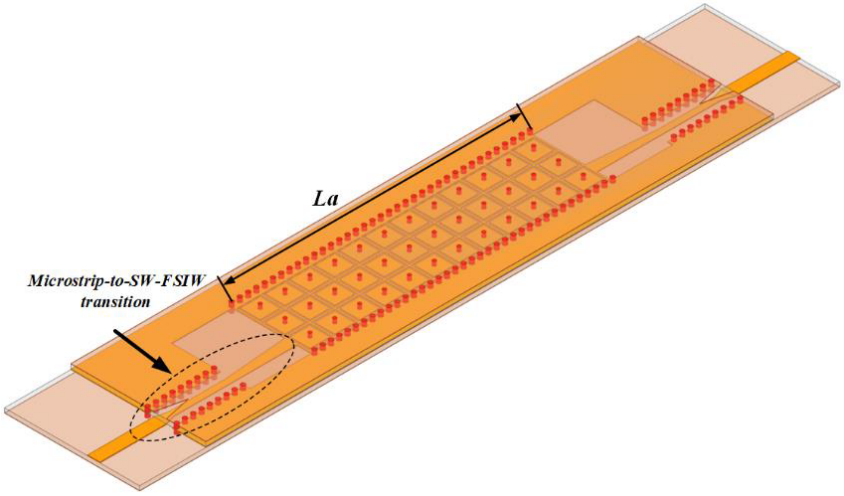

FIGURE 9. Configuration of the proposed SW-FSIW with microstrip-to-SW-FSIW transitions.

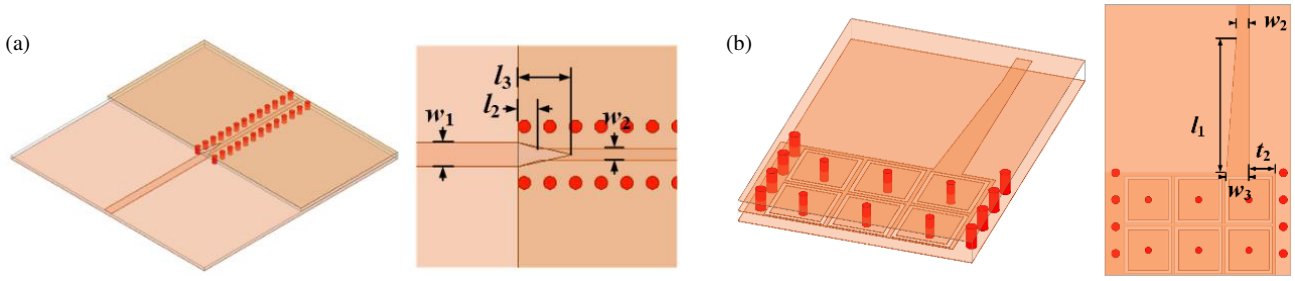

FIGURE 10. (a) Microstrip-to-stripline transition. (b) Stripline-to-SW-FSIW transmission.

TABLE 1. Dimensions of the fabricated SW-FSIW (Unit: mm).

W	d	l_1	w_1	d_1	t_2
10	0.4	8	2.4	0.5	1.55
g	w_2	w_3	a	s	p
0.2	0.75	1.45	3	0.2	1

3. EXPERIMENTAL RESULTS

Experimental validation was performed on fabricated prototypes of the proposed SW-FSIW structure with lengths of 36 mm and 72 mm. The measurement setup incorporated a custom-designed microstrip-to-SW-FSIW transition, optimized to achieve maximum bandwidth while maintain return loss better than 20 dB. As shown in Figure 9, this transition combines a microstrip-to-stripline section following

TABLE 2. Comparison with other SW-SIWs.

Ref.	Type	Lateral Reduction*	Longitudinal Reduction	Area Reduction	Fractional Bandwidth**	Attenuation Constant (dB/mm)	Processing Cost	No. of Layers
[12]	SIW with blind via-holes	40%	40%	64%	71.4%	0.03	High	2
[13]	SIW with antipodal blind via-holes	55%	50%	77.5%	21.6%	0.017	High	3
[14]	SIW with blind via-holes and patches	53%	75%	88.2%	90.2%	0.01	High	2
[15]	SIW with microstrip polylines	40%	40%	64%	73.9%	0.02	Low	1
[16]	SIW with lumped inductors	35%	35%	57.8%	66.7%	N/A	Medium	1
This Work	FSIW with through via-holes and patches	66%	37%	78.6%	>92%	0.008	Medium	2

*Compared with SIW with the same cutoff frequency. **Defined by $|S_{11}| < -10$ dB.

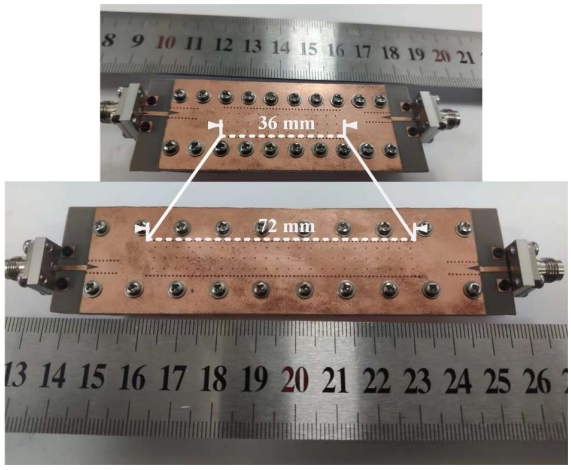

FIGURE 11. Photograph of the fabricated SW-FSIWs.

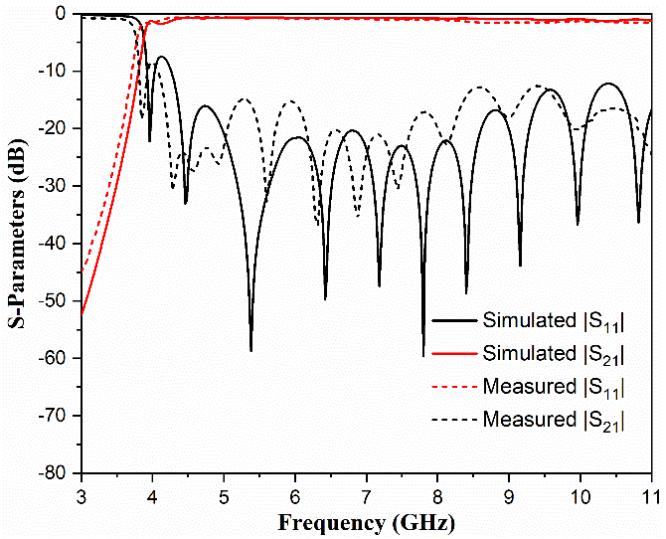

FIGURE 12. Simulated and measured S-parameters of the 72-mm-long SW-FIW with transitions.

established design principles [21] with an optimized stripline-to-waveguide interface (Figures 10(a) and (b)). All transition components were carefully dimensioned to maintain 50-Ω impedance matching, with the microstrip (w_4) and stripline (w_2) widths determined through parametric optimization. The complete set of final dimensions is provided in Table 1.

The fabricated devices (Figure 11) were manufactured using standard printed circuit board (PCB) processing techniques, with the two substrate layers aligned and secured using precision mechanical fasteners. Characterization measurements conducted with an Agilent PNA E8363C vector network analyzer revealed good correlation with simulation predictions, despite some expected variations. Figure 12 shows the simulated and measured results of the 72-mm-long SW-FSIW with microstrip-to-SW-FSIW transitions. The measured cutoff frequency of the SW-FSIW is 3.8 GHz, which is a little lower than the simulation. The measured return loss is better than 10 dB from 4.07 to 11 GHz, with a fractional bandwidth of 92%. The measured insertion loss of the SW-FSIW is lower than 1.1 dB, including the microstrip-to-SW-FSIW transitions. The slight

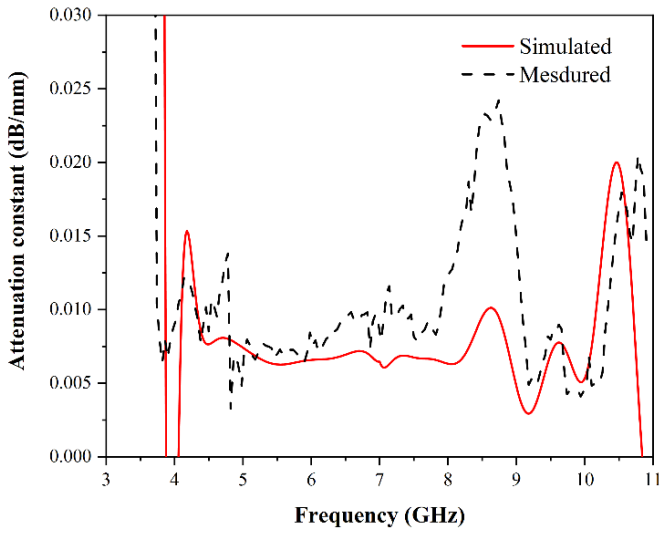

FIGURE 13. Simulated and measured attenuation constants of the SW-FSIW.

difference between the simulated and measured results may be caused by fabrication tolerance, the air gap between two substrate layers, and the permittivity fluctuation of the substrates. The intrinsic attenuation characteristics of the SW-FSIW itself, extracted using the methodology from [22], demonstrated an exceptionally low loss of 0.008 dB/mm (Figure 13). This performance, combined with the measured 66% lateral size reduction relative to conventional SIW designs, represents a significant advancement in slow-wave waveguide technology.

The comprehensive performance comparison presented in Table 2 highlights the design's advantages over existing approaches, particularly in achieving simultaneously wide bandwidth ($> 92\%$), low loss (0.008 dB/mm), and substantial miniaturization while maintaining practical fabrication requirements.

4. CONCLUSION

This paper proposes a novel slow-wave FSIW structure using ring-mushroom units, achieving 66% lateral size reduction and 37% phase velocity decrease versus conventional SIW. The design demonstrates superior performance with 92% bandwidth and 0.008 dB/mm loss while maintaining moderate fabrication cost. These advantages make it promising for developing compact microwave components in future work.

ACKNOWLEDGEMENT

This work was supported by the Science and Technology Program of Zhejiang Provincial Department of Transportation under Grant 2024012, "Pioneer" and "Leading Goose" R & D Program of Zhejiang under Grant 2023C03154, 2024 Zhejiang Provincial Human Resources and Social Security Research Project (No. 2024176).

REFERENCES

[1] Deslandes, D. and K. Wu, "Integrated microstrip and rectangular waveguide in planar form," *IEEE Microwave and Wireless Components Letters*, Vol. 11, No. 2, 68–70, Feb. 2001.

[2] Yan, X. and W. Mu, "Square-coupled topological filter with an ideal rectangular coefficient facilitated by dual-cavity single-mode and single-cavity dual-mode SIW resonators," *Progress In Electromagnetics Research Letters*, Vol. 122, 1–7, 2024.

[3] Che, W., L. Geng, K. Deng, and Y. L. Chow, "Analysis and experiments of compact folded substrate-integrated waveguide," *IEEE Transactions on Microwave Theory and Techniques*, Vol. 56, No. 1, 88–93, Jan. 2008.

[4] Zhu, F., X. Zhao, J. Sheng, and G. Q. Luo, "Broadband and compact folded substrate integrated waveguide phase shifter and its application to 180 directional coupler," *International Journal of Microwave and Wireless Technologies*, Vol. 15, No. 4, 554–559, 2023.

[5] Lai, Q., C. Fumeaux, W. Hong, and R. Vahldieck, "Characterization of the propagation properties of the half-mode substrate integrated waveguide," *IEEE Transactions on Microwave Theory and Techniques*, Vol. 57, No. 8, 1996–2004, Aug. 2009.

[6] Cherif, N., H. Chaker, M. Abri, F. Benzerga, H. Badaoui, J. Tao, T.-H. Vuong, and S. Ahmad, "A high pass filter based on half mode substrate integrated waveguide technology for cm waves," *Progress In Electromagnetics Research Letters*, Vol. 104, 149–154, 2022.

[7] Li, L., X. Yan, F. Wei, G. Liao, W. Yv, and K. He, "Miniaturized filter unit based on serpentine microstrip resonator and half-mode substrate integrated waveguide and its application," *Progress In Electromagnetics Research Letters*, Vol. 122, 93–99, 2024.

[8] Bozzi, M., S. A. Winkler, and K. Wu, "Broadband and compact ridge substrate-integrated waveguides," *IET Microwaves, Antennas & Propagation*, Vol. 4, No. 11, 1965–1973, 2010.

[9] Zhou, T., Y. Yin, W. Shen, Z. Yi, and T. Zhao, "A large-frequency-ratio filtering crossover based on ridged SIW resonators," *Progress In Electromagnetics Research Letters*, Vol. 123, 69–76, 2025.

[10] Chen, H., Y. Shao, J. Xiang, Z. He, and C. Zhang, "A wideband circularly polarized ridge substrate integrated waveguide (RSIW) endfire antenna," in *2021 IEEE International Symposium on Antennas and Propagation and USNC-URSI Radio Science Meeting (APS/URSI)*, 1197–1198, Singapore, 2021.

[11] Che, W., C. Li, P. Russer, and Y. L. Chow, "Propagation and band broadening effect of planar integrated ridged waveguide in multilayer dielectric substrates," in *2008 IEEE MTT-S International Microwave Symposium Digest*, 217–220, Atlanta, GA, USA, 2008.

[12] Niembro-Martin, A., V. Nasserddine, E. Pistono, H. Issa, A.-L. Franc, T.-P. Vuong, and P. Ferrari, "Slow-wave substrate integrated waveguide," *IEEE Transactions on Microwave Theory and Techniques*, Vol. 62, No. 8, 1625–1633, Aug. 2014.

[13] Zhou, Y., H. Jin, Y. M. Huang, D. Xu, S. Ding, P. Wang, M. Bozzi, and L. Perregrini, "Slow-wave effect enhanced substrate integrated waveguide with multi-antipodal blind via-holes and distributed metal strips," *IEEE Microwave and Wireless Components Letters*, Vol. 30, No. 8, 753–756, Aug. 2020.

[14] Zhang, Y., J.-Y. Deng, D. Sun, J.-Y. Yin, L.-X. Guo, X.-H. Ma, and Y. Hao, "Slow wave substrate-integrated waveguide with miniaturized dimensions and broadened bandwidth," *IEEE Transactions on Microwave Theory and Techniques*, Vol. 69, No. 8, 3675–3683, Aug. 2021.

[15] Jin, H., K. Wang, J. Guo, S. Ding, and K. Wu, "Slow-wave effect of substrate integrated waveguide patterned with microstrip polyline," *IEEE Transactions on Microwave Theory and Techniques*, Vol. 64, No. 6, 1717–1726, Jun. 2016.

[16] Jin, H., Y. Zhou, Y. M. Huang, and K. Wu, "Slow-wave propagation properties of substrate integrated waveguide based on anisotropic artificial material," *IEEE Transactions on Antennas and Propagation*, Vol. 65, No. 9, 4676–4683, Sep. 2017.

[17] Khalil, M., M. Kamarei, J. Jomaah, and H. Ayad, "Multilayer slow-wave half-mode substrate integrated waveguide," in *2015 International Conference on Microwave and Photonics (ICMAP)*, 1–2, Dhanbad, India, 2015.

[18] Jin, H., Y. Zhou, Y. M. Huang, S. Ding, and K. Wu, "Miniaturized broadband coupler made of slow-wave half-mode substrate integrated waveguide," *IEEE Microwave and Wireless Components Letters*, Vol. 27, No. 2, 132–134, Feb. 2017.

[19] Zhou, Y., Y. M. Huang, H. Jin, S. Ding, D. Xu, L. Silvestri, M. Bozzi, and L. Perregrini, "Slow-wave half-mode substrate integrated waveguide 3-dB Wilkinson power divider/combiner incorporating nonperiodic patterning," *IEEE Microwave and Wireless Components Letters*, Vol. 28, No. 9, 765–767, Sep. 2018.

[20] Ji, L., X. Li, Y. Zhu, H. Zhong, and J. Mao, "A miniaturized HMSIW-SPP guided-wave transmission line with mushroom-like structure," in *2019 IEEE Asia-Pacific Microwave Conference (APMC)*, 19–21, Singapore, Dec. 2019.

[21] Idury, S. K. and S. Mukherjee, "A wideband DC isolated substrate integrated coaxial line transition for system integration," in *2020 50th European Microwave Conference (EuMC)*, 731–734, Utrecht, Netherlands, 2021.

[22] Mangan, A. M., S. P. Voinigescu, M.-T. Yang, and M. Tazlauanu, "De-embedding transmission line measurements for accurate modeling of IC designs," *IEEE Transactions on Electron Devices*, Vol. 53, No. 2, 235–241, Feb. 2006.